Mon. Not. R. Astron. Soc. **386,** 1625–1634 (2008) doi:10.1111/j.1365-2966.2008.13143.x

The old open cluster NGC 2112: updated estimates of fundamental parameters based on a membership analysis⋆†

G. Carraro,[1,2,3,4]‡ S. Villanova,[2,5]‡ P. Demarque,[4]‡ C. Moni Bidin[3]‡ and M. V. McSwain[4,6]‡

[1]*ESO, Casilla 19001, Santiago 19, Chile*
[2]*Dipartimento di Astronomia, Università di Padova, vic. Osservatorio 3, Padova, Italy*
[3]*Departamento de Astronomia, Universidad de Chile, Casilla 36-D, Santiago, Chile*
[4]*Astronomy Department, Yale University, PO Box 208101 New Haven, CT 06520-8101, USA*
[5]*Departamento de Física, Facultad de Ciencias Físicas y Matemáticas Universidad de Concepción, Casilla 160-C, Concepción, Chile*
[6]*Department of Physics, Lehigh University, 16 Memorial Drive East, Bethlehem, PA 18015, USA*

Accepted 2008 February 21. Received 2008 February 20; in original form 2008 January 17

ABSTRACT

We report on a new, wide-field (20×20 arcmin^2), multicolour ($UBVI$), photometric campaign in the area of the nearby old open cluster NGC 2112. At the same time, we provide medium-resolution spectroscopy of 35 (and high-resolution of additional 5) red giant and turn-off stars. This material is analysed with the aim to update the fundamental parameters of this traditionally difficult cluster, which is very sparse and suffers from heavy field star contamination. Among the 40 stars with spectra, we identified 21 bona fide radial velocity members which allow us to put more solid constraints on the cluster's metal abundance, long suggested to be as low as the metallicity of globulars. As indicated earlier by us on a purely photometric basis, the cluster [Fe/H] abundance is slightly supersolar ([Fe/H] $= 0.16 \pm 0.03$) and close to the Hyades value, as inferred from a detailed abundance analysis of three of the five stars with higher resolution spectra. Abundance ratios are also marginally supersolar.

Based on this result, we revise the properties of NGC 2112 using stellar models from the Padova and Yale–Yonsei groups.

For this metal abundance, we find that the cluster's age, reddening and distance values are 1.8 Gyr, 0.60 mag and 940 pc, respectively. Both the Yale–Yonsei and Padova models predict the same values for the fundamental parameters within the errors.

Overall, NGC 2112 is a typical solar neighbourhood, thin-disc star cluster, sharing the same chemical properties of F-G stars and open clusters close to the Sun.

This investigation outlines the importance of a detailed membership analysis in the study of disc star clusters.

Key words: open clusters and associations: general – open clusters and associations: individual: NGC 2112.

1 INTRODUCTION

Gathering information on metal abundance and abundance ratios of many Galactic clusters located in different regions of the disc and with different ages is mandatory to study the chemical evolution of the Galactic disc. This, in turn, provides us with hints on the formation mechanism of the disc and its relation with the other major components of the Galaxy, the halo and bulge (Janes & Phelps 1994; Carraro, Ng & Portinari 1998).

However, a frequent, well-known problem in the study of open star clusters is the stellar contamination from the general Galactic disc field, which complicates the analysis of the colour–magnitude diagram (CMD). It also makes it difficult to derive fundamental cluster parameters, especially metallicity, when only a few stars are observed.

A notorious example in this context is the nearby old open cluster NGC 2112 (Collinder 76, C 0551-0031, OCL 509), which has a

⋆This paper includes data gathered with the 6.5 Magellan Telescopes, located at Las Campanas Observatory, Chile.
†The data discussed in this paper will be made available at the WEBDA open cluster data base http://www.univie.ac.at/webda, which is maintained by E. Paunzen and J.-C. Mermilliod.
‡E-mail: gcarraro@eso.org (GC); sandro.villanova@unipd.it (SV); demarque@astro.yale.edu (PD); mbidin@das.uchile.cl (CMB); mcswain@lehigh.edu(MVM)

reputation of suffering from heavy field star contamination (Brown et al. 1996), and for this reason its basic parameters remain poorly constrained.

The first investigation on NGC 2112 was carried out by Richtler (1985, hereafter R85), who obtained photographic BV photometry for about 80 stars down to $V = 15$. Although his photometry barely reaches the cluster turn-off (TO), he nevertheless drew attention to this probably old, so far neglected cluster, and he suggested that NGC 2112 has a reddening of ∼0.5 mag and lies ∼800 pc from the Sun. By analysing additional Stromgren photometry, he proposed that the cluster had to be very metal-poor ([Fe/H] as low as −1.4).

A more accurate and deeper analysis was performed a few years later by Richtler & Kaluzny (1989). They obtained BV CCD photometry for about 500 stars in a field of 200 arcmin^2. Additionally, they obtained moderate-resolution spectra for a handful of bright stars. Their conclusions were that the cluster was very contaminated by field stars. Nevertheless, they were able to strengthen the suggestions of R85 by confirming that the cluster is indeed old (3–5 Gyr), is located 700–800 pc from the Sun and has a reddening of $E(B-V) = 0.60$ mag. Lacking a membership analysis, no further information on the cluster metallicity was provided.

Photometry in the Washington system by Geisler (1987) and Geisler, Claria & Minniti (1991) seems to confirm the previous suggestions that NGC 2112 is very metal-poor ([Fe/H] as low as −1.3).

More recently, three spectroscopic campaigns have been carried out in the field of the cluster. Friel & Janes (1993, hereafter FJ93) present moderate-resolution spectra of six stars. Out of these, five are considered members, and an average [Fe/H] of -0.52 ± 0.21 has been found. This is significantly larger than all the previous determinations. Brown et al. (1996, hereafter BWGO96) used the Blanco Echelle on CTIO to obtain high-resolution spectroscopy of six stars. They accepted just one star as a definitive member, providing an even higher metal content value, [Fe/H] = −0.15, only slightly lower than the solar value. Finally, Mermilliod & Mayor (2007, hereafter MM07) enlarged the sample of spectroscopic members to 3, out of six stars observed with Coravel. They underlined the need to obtain radial velocities (RVs) for a larger sample down to $V \approx 14.5$ to better probe the shape of the red giant branch (RGB). At the same time, this would also provide much firmer metallicity estimates.

In Carraro, Barbon & Boschetti (2002) we reported a Jonhson *BVI* photometry of the cluster down to magnitude $V = 20$. Assuming the metal content found by BWGO96, we found a reddening of $E(B-V) = 0.63 \pm 0.14$, a distance of 850 ± 100 pc and an age of 2.0 ± 0.3 Gyr. We argued on a purely photometric basis that the metallicity cannot be much lower than BWGO96 value, and we stressed the need for a new, more detailed spectroscopic investigation of the cluster.

In this paper we attempt such an investigation by securing the deepest and widest field coverage multicolour (*UBVI*) photometry of NGC 2112 to date. At the same time, we provide moderate- and high-resolution spectroscopy of 40 stars. With these data at hand, we present robust and updated determinations of the cluster's basic properties.

2 OBSERVATIONS AND DATA REDUCTION

In this work we present photometry and spectroscopy in the field of NGC 2112 obtained with three different telescopes. For this reason, the details of data acquisition and reduction are presented in the next three subsections.

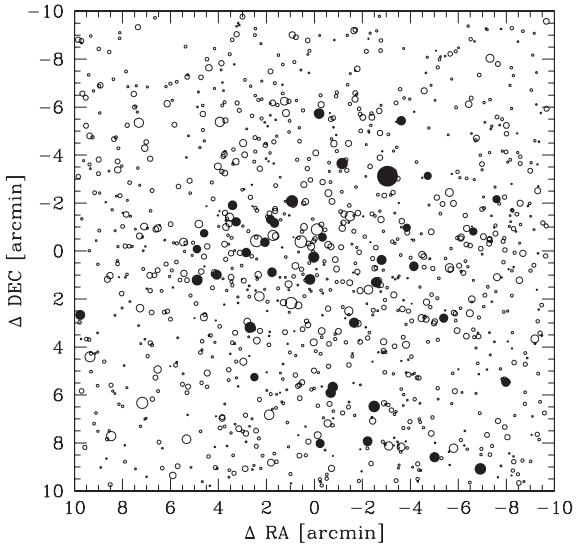

Figure 1. *V* filter map of the field covered by our photometry. Stars (empty circles) are plotted according to their magnitude. North is up and east is towards the left-hand side. The field is 20 arcmin on a side and centred at $(X, Y) = (2046, 2092)$ on star #593, which has $\alpha = 05{:}53{:}43.75$ and $\delta = +00{:}23{:}56.4$. With filled circles we indicate stars observed spectroscopically.

2.1 Photometry

U, B, V and I images centred on NGC 2112 were obtained at the Cerro Tololo Inter-American Observatory 1.0-m telescope, which is operated by the SMARTS[1] consortium. The telescope is equipped with a new 4000 × 4000 CCD camera having a pixel scale of 0.289 arcsec pixel^{-1}, which allows one to cover a field of 20 × 20 arcmin^2. This allows us to cover the entire cluster, which has an estimated diameter of 18 arcmin (Dias et al. 2002).

Observations were carried out on 2005 November 30. Three Landolt (1992) areas (TPhoenix, Rubin 149 and PG 0231+006) were also observed to calibrate the instrumental magnitudes to the standard system. The night was photometric with an average seeing of 1.1 arcsec. Data were reduced using IRAF[2] packages CCDRED, DAOPHOT and PHOTCAL. Photometry was done employing the point spread function (PSF) method (Stetson 1987). The covered area is shown in Fig. 1, while Table 1 contains the observational log.

The calibration equations read:

$$u = U + u_1 + u_2(U-B) + u_3 X \quad (1)$$

$$b = B + b_1 + b_2(B-V) + b_3 X \quad (2)$$

$$v = V + v_{1bv} + v_{2bv}(B-V) + v_3 X \quad (3)$$

$$v = V + v_{1vi} + v_{2vi}(V-I) + v_3 X \quad (4)$$

$$i = I + i_1 + i_2(V-I) + i_3 X \quad (5)$$

where *UBVI* are standard magnitudes, *ubvi* are the instrumental magnitudes, X is the airmass, and the derived coefficients are presented at the bottom of Table 1. To compute V magnitudes when B magnitudes were available, we use expression (3); otherwise we use expression (4). The standard stars in these fields provide a wide colour coverage with $-1.217 \leqslant (U-B) \leqslant 2.233$, $-0.298 \leqslant (B-V) \leqslant 1.999$ and $-0.361 \leqslant (V-I) \leqslant 2.268$. Aperture corrections

[1] http://www.astro.yale.edu/smarts/.

[2] IRAF is distributed by NOAO, which is operated by AURA under cooperative agreement with the NSF.

Table 1. Journal of photometric observations of NGC 2112 and standard star fields together with calibration coefficients (2005 November 30).

Field	Filter	Exposure time (s)	Seeing	Airmass (arcsec)
NGC 2112	*U*	1200, 60, 5	1.1	1.150–1.280
	B	900, 30, 3	1.0	1.150–1.280
	V	600, 30, 1	1.0	1.150–1.280
	I	600, 30, 1	1.0	1.150–1.280
TPhoenix	U	180, 200	1.0	1.024, 1.444
	B	90, 120	1.1	1.023, 1.447
	V	20, 30	1.1	1.024, 1.450
	I	40, 40	1.1	1.022, 1.452
PG 0231+006	U	200, 240	1.1	1.291, 1.801
	B	60, 90	1.1	1.293, 1.807
	V	40, 40	1.1	1.296, 1.809
	I	40, 30	1.1	1.294, 1.810
Rubin 149	U	180, 240	1.0	1.311, 1.651
	B	90, 120	1.1	1.316, 1.649
	V	30, 40	1.0	1.318, 1.647
	I	40, 40	1.0	1.313, 1.643
Calibration coefficients	$u_1 = +3.285 \pm 0.004$			
	$u_2 = +0.032 \pm 0.006$			
	$u_3 = +0.46$			
	$b_1 = +2.188 \pm 0.004$			
	$b_2 = -0.160 \pm 0.006$			
	$b_3 = +0.27$			
	$v_{1bv} = +2.188 \pm 0.014$			
	$i_1 = +2.789 \pm 0.044$			
	$i_2 = +0.021 \pm 0.043$			
	$v_{2bv} = +0.017 \pm 0.018$			
	$i_3 = +0.06$			
	$v_3 = +0.12$			
	$v_{1vi} = +2.188 \pm 0.016$			
	$v_{2vi} = +0.013 \pm 0.016$			

were estimated in a sample of 15 bright stars and then applied to all stars. They amounted to 0.315, 0.300, 0.280 and 0.280 mag for the *U*, *B*, *V* and *I* filters, respectively.

We cross-correlated our photometry with the photoelectric sequence of R85 to check our zero-points. The cross-identifications are listed in Table 2, where for comparison purposes we approximate our values to two digits, as in R85. Values that have not been measured either by R85 or by us are replaced with 99.999.

The differences in $V, B-V$ and $U-B$ between R85 and our study are illustrated in Fig. 2, and amount to

$\Delta V = 0.02 \pm 0.06$,

$\Delta(B-V) = 0.02 \pm 0.04$ and

$\Delta(U-B) = -0.01 \pm 0.09$.

Our photometry is basically consistent with R85. Only $U-B$, although in agreement, exhibits a significant scatter.

The resulting CMDs are shown in Fig. 3 for three colour combinations. The TO is located at $V \sim 14.5$, $(B-V) \sim 1.1$ and $(V-I) \sim 1.3$.

2.2 Spectroscopy: Hydra observations

Medium-resolution spectroscopic observations were carried out on the night of 2006 February 15 (Julian Date 245 3783.570 06) with the Hydra spectrograph onboard the Wisconsin Indiana Yale NOAO

Table 2. Comparison of our photometry with the photoelectric sequence of R85.

ID_{R85}	ID	V_{R85}	$(B-V)_{R85}$	$(U-B)_{R85}$	*V*	$(B-V)$	$(U-B)$
1-01	630	11.47	0.58	0.38	11.42	0.54	0.37
1-02	593	13.53	1.04	0.43	13.50	1.02	0.43
1-06	585	11.76	0.72	0.30	11.73	0.72	0.20
1-10	512	13.44	1.12	0.61	13.39	1.09	0.59
1-16	382	10.04	2.25	2.62			2.62
1-18	401	14.92	0.99	0.52	14.99	0.99	0.70
2-02	601	13.75	1.00	0.38	13.65	1.01	0.42
2-16	422	13.39	1.66	1.46	13.36	1.64	1.46
2-20	724	12.85	0.85	0.38	12.77	0.81	0.34
3-03	749	12.90	0.95	0.44	12.83	0.91	0.39
3-06	909	15.16	1.11	0.47	15.11	1.04	0.42
3-08	919	14.26	1.74		14.31	1.79	1.75
3-09	1029	14.12	1.22	0.60	14.05	1.17	0.72
3-10	935	13.52	1.68		13.54	1.62	1.38
3-16	1123	12.34	2.11	2.77	12.44	2.03	2.68
3-17	1026	11.79	2.15	2.64	11.80	2.07	2.49
3-18	954	13.42	1.49	1.01	13.31	1.55	1.05
4-01	711	12.30	1.51	1.17	12.38	1.56	1.35
4-02	759	11.47	1.47	1.15	11.43	1.42	1.10

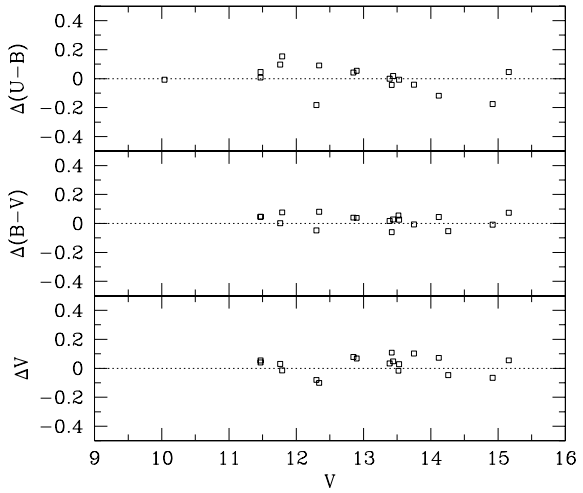

Figure 2. Comparison of our photometry with the R85 photoelectric sequence.

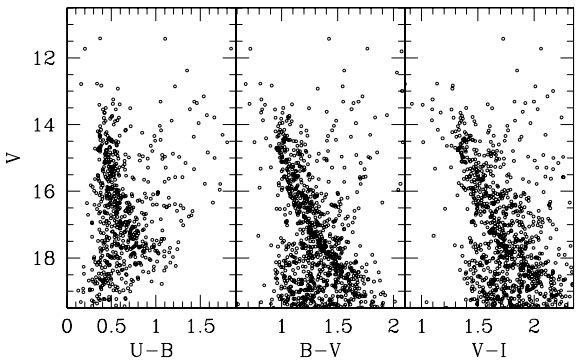

Figure 3. CMD for the stars in the field of NGC 2112 in the *V* versus $U-B$ (left-hand panel), *V* versus $B-V$ (middle panel) and *V* versus $V-I$ (right-hand panel).

(WIYN) telescope at Kitt Peak National Observatory under photometric conditions and typical seeing of 1.0 arcsec. The multi-object spectrograph consists of the Hydra positioner, which in 20 min can place 89 fibres within the 1° diameter focal plane of the telescope to 0.2 arcsec precision. This project employed the 3 arcsec diameter red-optimized fibre bundle.

The fibres feed a bench-mounted spectrograph in a thermally isolated room. With the echelle grating and the Bench Spectrograph Camera, the system produces a resolution of 15 000 at 6560 Å. The wavelength coverage of 400 Å around the central wavelength of 6560 Å provides a rich array of narrow absorption lines. We observed 35 TO–RGB stars with 2 × 45 min exposures, for a grand total of 1.5 h of actual photon collection time on each star.

The 35 stars were selected from the photometric catalogue presented in previous section. By using UCAC2 catalogue (Zacharias et al. 2004) as reference, we converted pixel coordinates into 2000.0 equinox right ascension (RA) and declination (Dec.) using 50 stars as input. The astrometry precision is 0.3 arcsec. The selected stars for Hydra are candidate RGB and TO stars according to their position in the CMD and have the right magnitudes to be observed with the WIYN 3.6-m telescope. We restricted the sample to stars brighter than $V \sim 15.0$. The stars are listed in Table 2, where column (1) reports numbering. In the following columns we report 2000.0 equinox coordinates, magnitude and colours, heliocentric RV and proper motion components from UCAC2 (Zacharias et al. 2004). In the last column an indication of membership is provided (see next section). For some stars (#782, 655, 890 and 417), no proper motions are available from UCAC2, probably because these stars have close companions.

Images were pre-reduced using IRAF[3] including bias subtraction, flat-field correction, frame combination, extraction of spectral orders, wavelength calibration, sky subtraction and spectral normalization. Some spectra turned out to have a very low signal-to-noise ratio (S/N), although all the observed stars have practically the same magnitude. This could happen for two reasons: the first is an imperfect pointing of the fibre, and the second is possibly bad fibre transmission.

2.3 Spectroscopy: MIKE observations

Echelle spectrograms of stars #535, #261, #717, #304 and #836 (see Table 2) were obtained on 2007 October 29 with the Magellan Inamori Kyocera Echelle (MIKE) spectrograph mounted on the Nasmyth focus of Landon Clay 6.5-m telescope at the Magellan Observatory. Data were obtained with both the blue and red arms. The slit was 0.7 arcsec wide, which yielded a resolution $R = 33\,000$, and the CCD was binned in steps of 2 pixels in the dispersion direction. The typical seeing was 0.6–0.8 arcsec. We used quartz lamp images without the diffuser in position for flat-field correction, and the wavelength calibration was performed with ThAr lamp images that were taken just before and after the five stellar exposures. The dark current was checked by examining several dark exposures and was found to be insignificant. The optimum algorithm (Horne 1986) was used to extract the spectra, which were also sky subtracted and normalized using IRAF routines. Additional details on the spectra are reported in Table 3.

3 MEMBERSHIP AND CLUSTER MEAN RADIAL VELOCITY

We derived RVs of the target stars using the IRAF fxcor task, which cross-correlates the object spectrum with a template. As a template, we used a synthetic spectrum calculated by SPECTRUM[4] with roughly the same atmospheric parameters and metallicity of the observed stars. The final errors in the RVs, as provided by fxcor, were typically less than 1.0 km s^{-1} for most of the Hydra stars and less than 0.3 km s^{-1} for MIKE targets (see Table 2). In the case of Hydra spectra, these have to be considered the real errors since they have been taken from the average of the two different exposures and their combined errors. In the case of MIKE spectra, having only one exposure, we consider the reported error as a lower limit of the real error.

The distribution of RVs is shown in the histogram in Fig. 4. The bulk of stars form a peak in the heliocentric RV distribution around 30–31 km s^{-1}, allowing us to define a mean velocity for the cluster and the dispersion, σ. These turn out to be

$$\mathrm{RV_H} = 30.9 \pm 0.4\ \mathrm{km\,s^{-1}}. \quad (1)$$

To derive this value we used 21 stars, which are listed in Table 2 as cluster members. These stars were selected using an interactive procedure in which we calculated an initial value for $\mathrm{RV_H}$ and σ. Then stars having RVs more than 3σ from the mean were rejected as non-members and a new value of $\mathrm{RV_H}$ and σ were computed. This procedure was iterated until no more stars were rejected.

It is, however, possible that some of the rejected stars are binary stars.

In Table 4, we compare our measurements with literature values. RV data for NGC 2112 are poor and very inhomogeneous. We have three stars in common with BWGO96, one with FJ93 and two with MM07. In all cases, the RVs are compatible within the errors, as are the membership assignments.

We confirm the result of BWGO96 that star #2-4 (our star 656) is a member.

One more star, for which we do not have new RV, can be considered a member, following MM07, if it is a binary: this is star #3-18 (our 954).

Finally, we find that #3-16, 4-1 and 4-2 (our stars 1123, 711 and 759) are member stars following the analysis in MM07 and looking at Table 5.

We make use of the CMD to get additional information on the cluster membership. In Fig. 5, we indicate with filled circles (red when printed in colour) the RV members, and with filled triangles (black when printed in colour) the RV non-members. Additionally, we plot as filled squares (blue in colour) stars that are members, but for which we do not have RV measurements (1123, 711 and 759), and star 362 (#3-16), for which we have measured its RV but not photometry, which we take from R85.

Clearly, members and non-members mix up in a way that, without RVs, it would not be possible to discriminate between them. Our member stars are partly located in the TO region and partly trace the subgiant branch and RGB of the cluster.

Among this membership sample, we find two stars with the radial velocities typical of members but located far from the most important loci in the CMD. They are stars #323 at $(V, B - V) = (14.896, 1.161)$ and #782 at (13.510, 1.244). We suggest that these stars may

[3] IRAF is distributed by the National Optical Astronomy Observatory, which is operated by the Association of Universities for Research in Astronomy, Inc., under cooperative agreement with the National Science Foundation.

[4] SPECTRUM is the local thermodynamic equilibrium (LTE) spectral synthesis program freely distributed by Richard O. Gray. See http://www.phys.appstate.edu/spectrum/spectrum.html.

Table 3. Basic properties of the stars for which we secured spectroscopic observations. In the last column, M indicates members according to radial velocity, NM indicates non-members.

ID	RA (hh:mm:ss)	Dec. (○:′:″)	U	B	V	σV	I	RV_H (km s^{-1})	$\mu_\alpha \cos\delta$ (mas yr^{-1})	μ_δ (mas yr^{-1})	
						Hydra observations					
101	05:53:11.7	+00:18:43.4	17.409	15.983	14.363	0.017	12.476	42.47 ± 0.68	3.6 ± 7.9	−10.8 ± 8.2	NM
124	05:53:13.2	+00:26:20.9	17.397	16.204	14.873	0.016	13.226	−3.16 ± 0.78	2.7 ± 8.1	−11.0 ± 7.8	NM
167	05:53:16.0	+00:15:06.6	16.433	15.000	13.313	0.018	11.315	29.60 ± 0.40	−3.6 ± 7.9	8.8 ± 7.8	M
185	05:53:17.1	+00:25:00.3	16.269	15.834	14.852	0.015	13.501	36.53 ± 0.96	−3.6 ± 7.8	−3.2 ± 7.8	NM
244	05:53:22.1	+00:21:23.7	15.913	15.433	14.407	0.015	13.026	32.02 ± 0.82	−2.4 ± 7.9	−2.8 ± 7.9	M
274	05:53:24.7	+00:27:19.5	16.907	16.094	14.909	0.016	13.247	−15.67 ± 1.62	−3.5 ± 7.8	4.2 ± 7.9	NM
323	05:53:28.2	+00:25:09.8	16.715	16.057	14.896	0.016	13.305	30.69 ± 1.90	−7.5 ± 7.8	3.0 ± 7.9	M
340	05:53:29.1	+00:29:37.5	16.264	15.418	14.246	0.016	12.655	32.27 ± 0.74	−10.1 ± 7.9	2.9 ± 7.9	M
382	05:53:31.4	+00:27:18.7	14.876	12.249				−6.18 ± 0.22	−1.2 ± 1.0	−7.5 ± 1.1	NM
399	05:53:32.4	+00:23:49.2	15.600	15.073	13.998	0.016	12.518	28.39 ± 0.60	−0.3 ± 7.8	5.5 ± 7.8	M
417	05:53:33.3	+00:22:53.3	16.547	15.369	13.882	0.017	12.052	29.49 ± 0.25			M
422	05:53:33.7	+00:17:42.9	16.461	15.000	13.357	0.018	11.435	−29.32 ± 0.26	−6.3 ± 7.8	−15.1 ± 7.8	NM
443	05:53:34.8	+00:16:16.0	16.550	15.505	14.037	0.016	12.275	29.52 ± 0.34	−5.9 ± 7.8	4.1 ± 7.9	M
478	05:53:37.0	+00:21:12.5	15.528	14.988	13.898	0.016	12.428	30.45 ± 0.44	1.2 ± 7.8	4.4 ± 7.8	M
512	05:53:39.0	+00:27:50.7	15.077	14.485	13.392	0.019	11.805	21.42 ± 1.52	−0.9 ± 7.8	−7.9 ± 7.8	NM
542	05:53:40.9	+00:18:17.1	15.307	14.820	13.824	0.015	12.458	30.78 ± 0.54	−1.8 ± 7.9	0.9 ± 7.8	M
566	05:53:42.3	+00:24:46.2	16.006	15.561	14.539	0.015	13.141	30.03 ± 0.67	−2.1 ± 7.8	−2.8 ± 7.9	M
577	05:53:42.7	+00:16:10.3	16.016	15.512	14.454	0.015	13.036	27.55 ± 0.65	−2.1 ± 7.9	5.1 ± 8.0	NM
580	05:53:42.8	+00:29:55.3	15.317	14.807	13.739	0.016	12.380	−12.84 ± 0.67	10.8 ± 7.9	0.2 ± 7.9	NM
593	05:53:43.7	+00:23:56.5	14.953	14.517	13.502	0.017	12.105	44.78 ± 0.49	−15.3 ± 7.8	−2.0 ± 7.8	NM
601	05:53:44.4	+00:23:00.7	15.076	14.654	13.647	0.019	12.302	30.02 ± 0.60	1.0 ± 7.8	−5.4 ± 7.8	M
655	05:53:47.3	+00:26:16.6	16.416	14.877	13.155	0.018	11.036	31.55 ± 0.21			M
656	05:53:47.5	+00:22:01.6	15.337	13.491	11.724	0.019	9.663	29.53 ± 0.27	3.2 ± 1.7	−0.8 ± 1.7	M
707	05:53:50.3	+00:25:22.1	15.495	15.148	14.202	0.015	12.900	30.81 ± 0.81	−9.2 ± 8.0	27.3 ± 7.9	M
714	05:53:50.7	+00:23:18.7	15.672	15.226	14.227	0.015	12.843	31.95 ± 0.70	1.9 ± 7.8	1.1 ± 7.9	M
737	05:53:51.9	+00:24:33.8	15.526	15.143	14.157	0.015	12.825	31.81 ± 0.57	−1.7 ± 7.8	−6.2 ± 8.0	M
770	05:53:53.6	+00:18:56.4	16.235	15.794	14.767	0.015	13.379	24.37 ± 0.86	1.7 ± 7.8	−5.8 ± 7.9	NM
782	05:53:54.3	+00:21:01.0	15.466	14.754	13.510	0.017	11.883	31.41 ± 0.24			M
794	05:53:55.0	+00:24:08.0	15.727	15.293	14.280	0.015	12.884	20.71 ± 0.57	3.0 ± 7.8	5.5 ± 8.1	NM
824	05:53:56.6	+00:25:24.8	15.698	15.327	14.366	0.015	13.056	30.65 ± 0.58	−0.9 ± 7.8	3.8 ± 7.9	M
890	05:53:59.9	+00:23:12.4	15.393	15.019	14.051	0.015	12.728	12.00 ± 0.53			NM
917	05:54:02.0	+00:24:56.4	16.075	15.724	14.757	0.016	13.436	22.70 ± 1.16	−12.0 ± 7.8	0.2 ± 8.2	NM
935	05:54:03.1	+00:22:59.5	16.546	15.162	13.537	0.018	11.505	38.33 ± 0.22	1.0 ± 7.8	−4.3 ± 7.8	NM
936	05:54:03.2	+00:24:16.8	15.987	15.671	14.719	0.015	13.384	−26.71 ± 1.81	−12.9 ± 7.8	4.2 ± 7.8	NM
1140	05:54:22.6	+00:21:32.6		14.947	13.964	0.021	12.581	3.89 ± 1.01	−1.0 ± 7.8	3.3 ± 7.9	NM
						MIKE observations					
261	05:53:23.6	+00:15:35.9	17.100	15.619	13.955	0.015	11.987	19.84 ± 0.14	−6.3 ± 7.8	−6.7 ± 7.9	NM
304	05:53:27.1	+00:23:33.3	16.059	15.402	14.181	0.015	12.583	29.27 ± 0.15	−4.2 ± 7.8	−0.6 ± 7.9	M
535	05:53:40.6	+00:18:31.4	15.326	14.826	13.770	0.017	12.317	29.55 ± 0.25	2.7 ± 7.9	−1.9 ± 7.9	M
717	05:53:50.9	+00:25:30.8	15.676	15.308	14.336	0.012	12.998	39.03 ± 0.24	4.1 ± 7.9	0.6 ± 7.9	NM
836	05:53:57.3	+00:26:06.1	16.681	15.622	14.171	0.014	12.402	29.26 ± 0.16	−6.1 ± 8.1	3.2 ± 7.9	M

be binary members, as is star #3-18 (our 954, see MM07), which must be confirmed by future studies (but see Section 7 for additional details). Unfortunately, we cannot use proper motions (see Table 2) to improve our membership assignments due to the large associated errors.

4 ABUNDANCE MEASUREMENTS

4.1 Atomic parameters and equivalent widths

We performed the analysis of chemical abundances on the three members observed with MIKE using the 2007 version of the freely available program MOOG developed by Chris Sneden[5] and using model atmospheres by Kurucz (1992). MOOG performs an LTE analysis. We derived equivalent widths of spectral lines by Gaussian fitting of spectral features. Repeated measurements show a typical error of about 5 mÅ for the weakest lines. The line list was taken from Carraro et al. (2008). The log(gf) parameters of these lines were redetermined by a solar-inverse analysis measuring the equivalent widths from the NOAO solar spectrum (Kurucz et al. 1984), adopting standard solar parameters ($T_{\rm eff}$ = 5777 K, log (g) = 4.44 and $v_{\rm t}$ = 0.8 km s^{-1}). The O abundance was obtained from the infrared triplet at 7771–7775 Å, while the Na abundance was obtained from the spectral doublets at 5662–5668 and 6154–6160 Å. These features are well known to be affected by non-LTE (NLTE) effects. For this reason we applied NLTE correction to the output LTE abundances, obtained from Gratton et al. (1999).

[5] http://verdi.as.utexas.edu/moog.html.

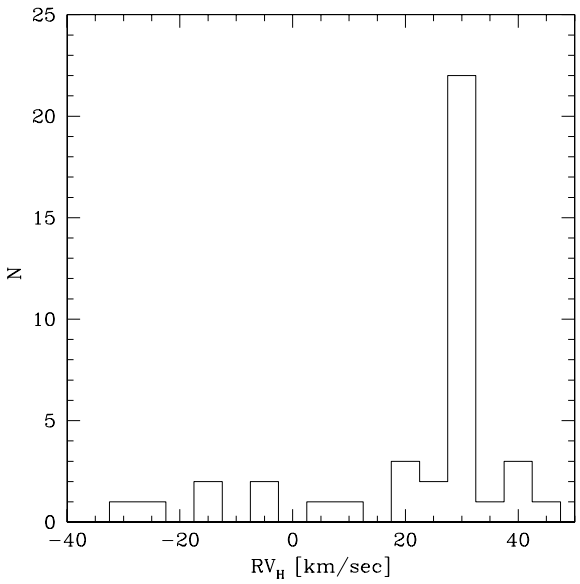

Figure 4. Distribution of radial velocities from the present study.

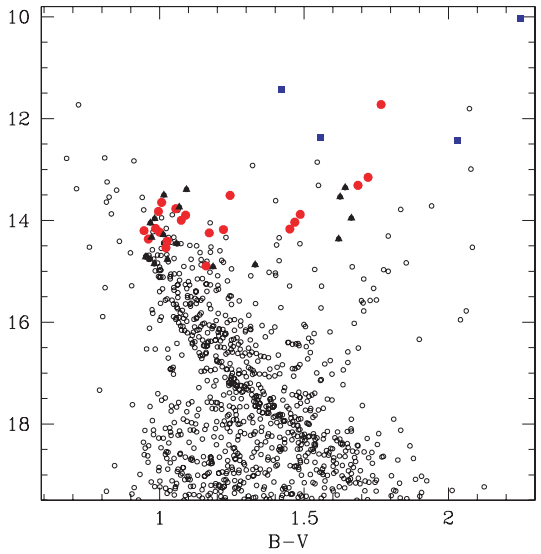

Figure 5. CMD of NGC 2112. Filled circles (red when printed in colour) indicate radial velocity members, while filled triangles (black in colour) non-members. Filled (colour coded in blue) squares are member stars for which we do not have either photometry or radial velocity. See text for additional details.

Table 4. Observational details of the five stars observed with MIKE.

ID	Julian Date	Exposure time (s)	S/N
535	245 4303.823 17	500	80
261	245 4403.816 00	800	60
717	245 4403.835 38	1200	100
304	245 4403.850 79	1600	90
836	245 4403.870 42	1300	80

Table 5. Radial velocity: comparison with literature data.

R85	ID	V	$(B-V)$	RV$_H$	BWGO96	FJ93	MM07
1-16	382			-6.18 ± 0.22	-3.6		-4.04
2-4	656	11.724	1.767	29.53 ± 0.27	30.04		
2-16	422	13.357	1.643	-29.32 ± 0.26	-23.3	-22	-29.02
3-16	1123	12.441	2.030			21	31.75
3-17	1026	11.805	2.073			40	44.76
3-18	954	13.312	1.550		25.3		
4-1	711	12.380	1.639				28.56
4-2	759	11.429	1.423		21.6–30.1	35	32.53
4-16	883	12.856	1.546		44.5	60	

4.2 Atmospheric parameters

Initial estimates of the atmospheric parameter $T_{\rm eff}$ were obtained from photometric observations using the relations from Alonso, Arribas & Martínez-Roger (1999). We adopted $E(B-V)$ values from Carraro et al. (2002) to correct colours for interstellar extinction. We then adjusted the effective temperature by minimizing the slope of the abundances obtained from Fe I lines with respect to the excitation potential in the curve of growth analysis. Initial guesses for the gravity log (g) were derived from the canonical formula:

$$\log\left(\frac{g}{g_\odot}\right) = \log\left(\frac{M}{M_\odot}\right) + 4\log\left(\frac{T_{\rm eff}}{T_\odot}\right) - \log\left(\frac{L}{L_\odot}\right). \quad (2)$$

Table 6. Atmospheric parameters of MIKE member stars.

ID	$T_{\rm eff}$ (K)	log(g)	v_t (km s^{-1})	[Fe/H]
535	6650	3.85	1.70	0.15 ± 0.02
304	5980	3.65	1.00	0.19 ± 0.02
836	5130	3.48	1.02	0.13 ± 0.01

In this equation, the mass $M/M_\odot$ was derived from the comparison between the position of the star in the Hertzsprung–Russell diagram and the Padova isochrones (Girardi et al. 2000). The luminosity $L/L_\odot$ was derived from the absolute magnitude M_V, assuming a distance moduli of $(m-M)_V = 11.6$. The bolometric correction (BC) was derived from the BC-Teff relation from Alonso et al. (1999). The input log(g) values were then adjusted in order to satisfy the ionization equilibrium of Fe I and Fe II during the abundance analysis. Finally, the microturbulence velocity is given by the relation (Houdashelt, Bell & Sweigart 2000)

$$v_t = 2.22 - 0.322\log(g). \quad (3)$$

We then adjusted the microturbulence velocity by minimizing the slope of the abundances obtained from Fe I lines with respect to the equivalent width in the curve of growth analysis. The adopted values for all these parameters, together with [Fe/H], are reported in Table 6. The results of the abundance analysis are listed in Table 7, where the abundances of the main elements are reported with their uncertainties. Two stars turn out to be giants (#304 and 836), while star #535 is clearly a dwarf. This explains the different number of lines used in the determination of the different elemental abundances.

As a final remark, we also performed an abundance analysis for the two RV non-members, and found that the two stars #261 and #717 have [Fe/H] $= +0.28 \pm 0.02$ and $+0.30 \pm 0.03$, confirming their nature as non-member stars.

Examples of our extracted spectra are illustrated in Fig. 6, in which the spectrum of three MIKE member stars are shown and some interesting lines indicated.

Table 7. Abundance analysis from MIKE cluster members. After each value, in parenthesis, the number of lines *N* used is indicated. Values derived from just one line do not have any error associated.

Element	#535	*N*	#304	*N*	#836	*N*
[Fe/H]	0.15 ± 0.02	(19)	0.19 ± 0.02	(71)	0.13 ± 0.01	(107)
$[O/H]_{LTE}$	0.45 ± 0.07	(3)	0.36 ± 0.01	(3)	0.27 ± 0.03	(3)
$[O/H]_{NLTE}$	0.03 ± 0.07	(3)	0.17 ± 0.01	(3)	0.23 ± 0.03	(3)
$[Na/H]_{LTE}$	0.35 ± 0.13	(2)	0.20 ± 0.06	(4)	0.30 ± 0.06	(3)
$[Na/H]_{NLTE}$	0.24 ± 0.13	(2)	0.15 ± 0.06	(4)	0.23 ± 0.06	(3)
[Mg/H]	0.13	(1)	0.18	(1)	0.27 ± 0.03	(2)
[Al/H]			0.10 ± 0.09	(2)	0.05 ± 0.03	(3)
[Si/H]	0.33 ± 0.02	(3)	0.11 ± 0.06	(5)	0.11 ± 0.05	(8)
[Ca/H]	0.18 ± 0.07	(7)	0.23 ± 0.04	(13)	0.07 ± 0.05	(13)
[Ti/H]	0.20 ± 0.04	(2)	0.43 ± 0.09	(7)	0.23 ± 0.04	(23)
[V/H]			-0.01	(1)	0.31 ± 0.06	(10)
[Cr/H]	0.51 ± 0.05	(2)	0.41 ± 0.08	(6)	0.14 ± 0.03	(11)
[Mn/H]	-0.18	(1)	0.03 ± 0.03	(3)	0.10 ± 0.02	(3)
[Co/H]			0.27 ± 0.07	(2)	0.24 ± 0.06	(4)
[Ni/H]	0.17	(1)	0.24 ± 0.05	(15)	0.21 ± 0.03	(29)
[Cu/H]			0.38	(1)	0.12	(1)
[Y/H]			0.45	(1)	0.51 ± 0.24	(2)
[Ba/H]	0.59	(1)	0.84 ± 0.06	(2)	0.40 ± 0.01	(2)

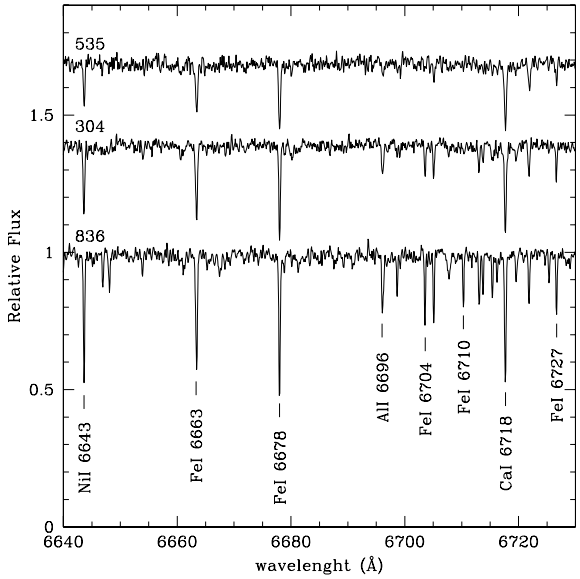

Figure 6. Extracted spectra for the three MIKE member stars. A few important lines are indicated.

The mean metallicity we derive ([Fe/H] $= +0.16 \pm 0.03$) is significantly different from any previous spectroscopic estimate. The closest determination is the one by BWGO96, who found [Fe/H] $= -0.15 \pm 0.15$. Our result rules out any possibility that NGC 2112 is very metal-poor, as suggested in early studies. It would have been very unusual to have such a metal-poor cluster in the solar neighbourhood. Our result, in fact, suggests that NGC 2112 has a typical solar vicinity metal abundance, being as metal-rich as the Hyades (Boesgaard & Friel 1990).

Karatas & Schuster (2006) provided a new calibration of the relation between the metallicity of a dwarf star and $\delta_{0.6}$, namely the $(U - B)$ excess/deficiency with respect to the Haydes sequence at $(B - V)_0 = 0.6$. We compared the distribution of dwarf stars in NGC 2112 at $(B - V)_0 \sim 0.6$ with respect to a zero-age main-sequence (ZAMS) from Girardi et al. (2000) having the same metallicity of the Hyades ([Fe/H] $= 0.17$). We found that the useful stars (13 in number) have $\delta_{0.6} = -0.02 \pm 0.11$. Despite the scatter, this $\delta_{0.6}$ implies a metallicity close to our spectroscopic determination (see Table 3).

5 ABUNDANCE RATIOS

We derived abundance ratios for the three MIKE member stars listed in Table 7. Previously, only BWGO96 provided an estimate of a few abundance ratios in NGC 2112, but based on just one star. At any rate, we compare our findings with BWGO96 (their table 6), and find basic agreement with [O/Fe] and [Na/Fe]. However, their [Al/Fe] is much larger than our value.

Being close to the Sun and having roughly the same metallicity, it is useful to make a detailed comparison of the chemical properties of NGC 2112 with the solar neighbourhood stars and star clusters.

5.1 Comparison with field stars

Bensby et al. (2005) present a detailed abundance analysis for a sample of 102 F and G dwarf stars in the solar vicinity.

α-elements: As shown by Bensby et al. (2005), O, Mg, Si, Ca and Ti exhibit similar trends in the Galactic thin disc. At the Fe abundance of NGC 2112 (+0.16), these ratios are in the range of −0.15:0.00, 0.00:+0.15, 0.00:+0.15, 0.00:+0.15 and −0.05:0.05 dex, respectively.

According to our findings, abundance ratios for these five elements in NGC 2112 are in agreement with the thin-disc values within the errors. This confirms that NGC 2112 is a typical thin-disc star cluster. The overall [α/Fe] ratio turns out to be 0.04 ± 0.03.

Iron peak elements: We can compare only Ni and Cr with Bensby et al. (2005). Ni is basically in agreement with the thin-disc trends, whereas the [Cr/Fe] ratio is marginally overabundant.

Al and Na: While the Na abundance relative to Fe is consistent with thin-disc values, we find that Al is significantly underabundant.

r- and s-process elements: We measured Y and Ba abundance ratios. While the Ba abundance in NGC 2112 is consistent with the thin-disc trend, we find that the Y abundance is significantly larger than typical thin-disc values.

5.2 Comparison with open clusters

In general, there is not much information on abundance ratios in open clusters, and only in the last few years efforts have been made to improve this situation.

Here, we compare our NGC 2112 abundance ratios with the results presented in Friel et al. (2003). They provide a detailed abundance analysis of the old star cluster Collinder 261 and compare its abundance ratios with a sample of 10 open clusters (see their table 7). From this table, we extract estimates for NGC 2360 and 6819, two nearby clusters having roughly the same ages and metal abundances as NGC 2112. We find that within the errors, NGC 2360 and 6819 possess the same [α/Fe] as NGC 2112, +0.03 and 0.00, respectively.

The Na abundance of NGC 2112 is similar to NGC 2360 but significantly lower than in NGC 6819. As for Al, we can make a comparison only with NGC 6819, for which [Al/Fe] is similar to the value we determine for NGC 2112.

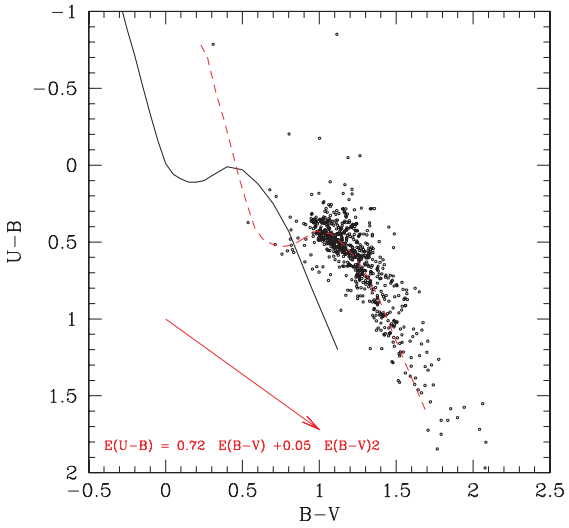

Figure 7. Two-colour diagram for NGC 2112 stars. The solid line is the Schmidt-Kaler (1982) empirical ZAMS and the dashed line is the same ZAMS shifted by $E(B-V) = 0.60$ along the reddening vector (the arrow) for a normal reddening law.

Unfortunately, information about neither the iron-peak elements nor s- and r-process elements are reported in Friel et al. (2003).

Overall, with a few exceptions, we find that NGC 2112 is a genuine thin-disc population cluster.

6 CLUSTER FUNDAMENTAL PARAMETERS

Having an estimate of the metal content ([Fe/H] = +0.16), and of the α-element abundances ([α/Fe] = +0.04), we are now in the position to derive more reliable estimates of the cluster parameters.

The reddening value in the direction of NGC 2112 predicted by Schlegel, Finkbeiner & Davis (1998) maps is $E(B-V) = 1.01$. This has to be considered as an upper limit to the reddening since it takes into accounts the absorption all the way to infinity.

To get an independent estimate of the reddening in the direction of NGC 2112, we make use of the two-colour diagram in Fig. 7 since we provide deep *U*-band photometry for the first time. Here, the solid line is the zero reddening empirical ZAMS from Schmidt-Kaler (1982). The same ZAMS, shifted by $E(B-V) = 0.60$ is shown as a dashed line. The shift has been performed adopting the standard reddening law (see the expression in the bottom of Fig. 7), and the reddening vector is indicated with a solid arrow.

We compare the distribution of stars in the various colour combination CMDs and sets of theoretical Padova (Girardi et al.

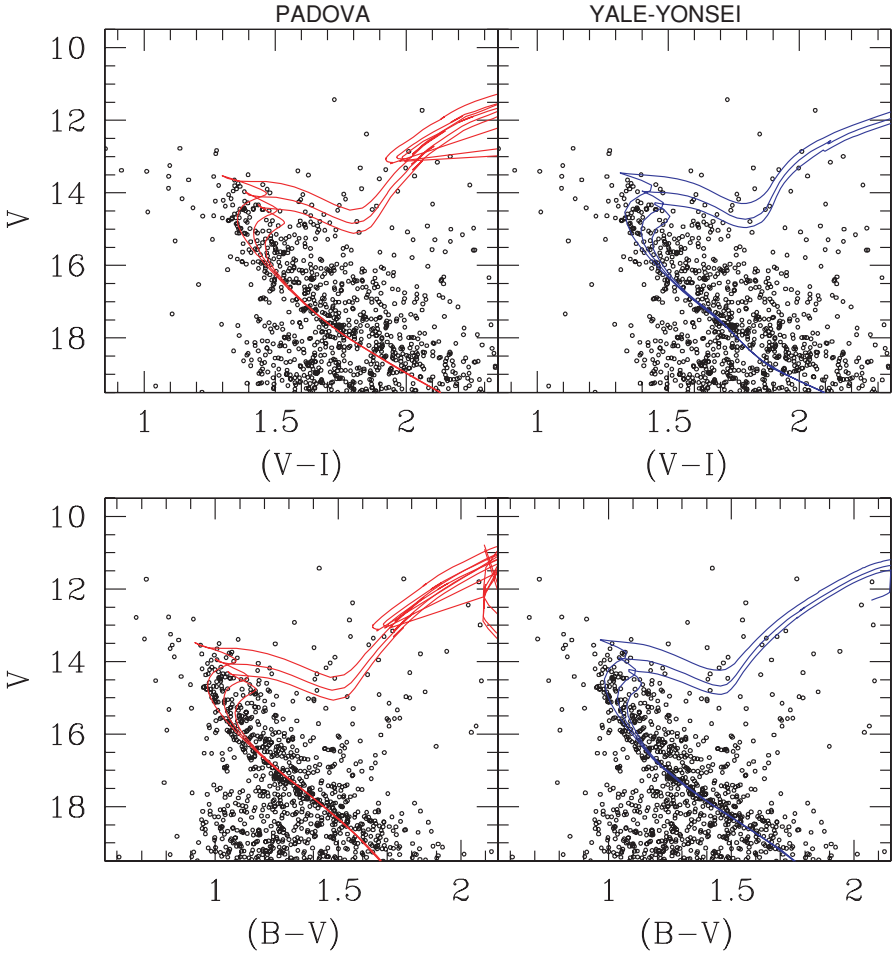

Figure 8. Isochrone fits for the derived metallicity and varying ages. Bottom panels show the fits in the *V* versus $(B-V)$ plane, upper panels show the fits in the *V* versus $(V-I)$ plane. Left-hand panels refer to Padova isochrones and right-hand panels refer to Yale–Yonsei isochrones.

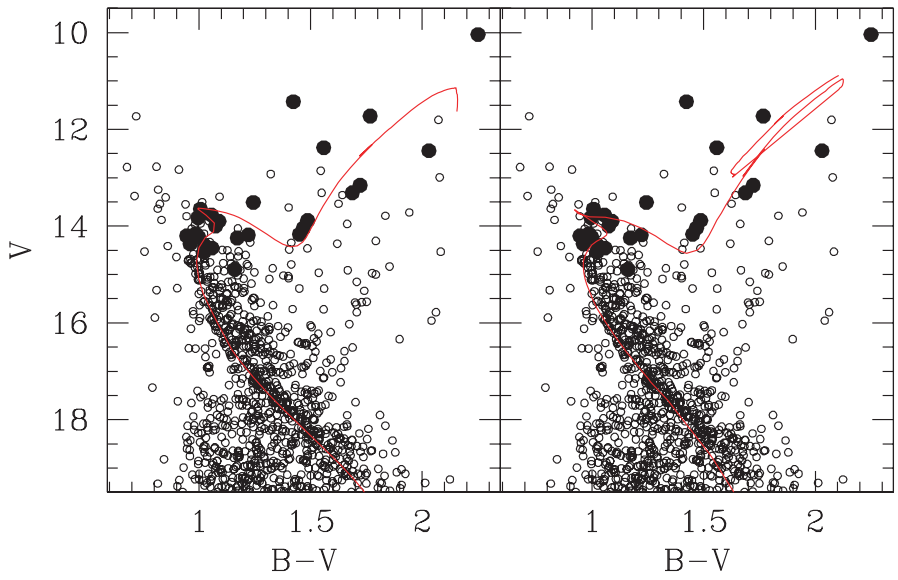

Figure 9. The best-fitting isochrone is superimposed on the NGC 2112 CMD where radial velocity members are indicated with solid circles. Left-hand panel refers to Yale–Yonsei isochrones and the right-hand panel refer to Padova isochrones. The isochrones have been adjusted using the values listed in Table 8.

2000) and Yale (Yi et al. 2001; Kim, Demarque & Alexander 2002; Demarque et al. 2004) isochrones. The physical ingredients of the two sets, and the possible sources of different results, have been discussed exhaustively in Carraro et al. (2006), where a similar exercise has been done for the very metal-rich open cluster NGC 6791.

In Fig. 8 we superimpose isochrones with [Fe/H] = +0.16 and [α/Fe] = +0.04 for three ages (1.5, 2.0 and 2.5 Gyr). The fitting is performed in the left-hand panels for Padova models, and in the right-hand panels for Yale models.

To derive more constrained basic parameters, we consider in Fig. 9 the star distribution in the V versus $(B - V)$ plane, and we highlight the RV members using filled circles. The best-fitting isochrone is found for an age of 1.8 $\pm$ 0.3 Gyr, where the associate error has been derived by trying different age isochrones.

We find that the both the Yale–Yonsei and Padova sets fit the star distribution well, and we summarize the derived values for the basic parameters in Table 8.

On average, we obtained $(m - M)_V = 11.75 \pm 0.15$ and $E(B - V) = 0.60 \pm 0.10$. The errors here reported have been derived by displacing the best-fitting isochrone back and forth in the distance modulus and reddening directions and exploring the values of distance modulus and reddening which produce acceptable fits (see Table 9).

The two sets of models imply the same values for NGC 2112 basic parameters within the errors. It is worth noting, however, that the fit implies a sizeable difference in the mean $E(B - V)$, in the sense that the reddening that inferred using Yale–Yonsei models is larger than that inferred from Padova models. At the same age and metal abundance, the apparent Yale–Yonsei RGB is bluer than the Padova one, resulting in a larger reddening when fitting the observed RGB.

Using the heliocentric rectangular Galactic coordinates X = 9.3 kpc, Y = −400 pc, and Z = −200 pc and assuming the Sun distance from the Galactic Centre is 8.5 kpc, NGC 2112 is located 940 $\pm$ 70 pc from the Sun towards the anticentre direction. Consequently, we infer a distance of 9.3 kpc from the Galactic Centre.

Table 8. Abundance ratios from MIKE cluster members.

Element	#535	#304	#836
$[O/Fe]_{NLTE}$	−0.12	−0.02	0.10
$[Na/Fe]_{[NLTE]}$	0.09	−0.04	0.10
[Mg/Fe]	−0.02	−0.01	0.14
[Al/Fe]		−0.09	−0.08
[Si/Fe]	0.18	−0.08	−0.02
[Ca/Fe]	0.03	0.04	−0.06
[Ti/Fe]	0.05	0.24	0.10
[V/Fe]		−0.20	0.18
[Cr/Fe]	0.36	0.22	0.01
[Mn/Fe]	−0.33	−0.16	−0.03
[Co/Fe]		0.08	0.11
[Ni/Fe]	0.02	0.05	0.08
[Cu/Fe]		0.19	−0.01
[Y/Fe]		0.26	0.38
[Ba/Fe]	0.44	0.65	0.27

Table 9. Summary of NGC 2112 fundamental parameters derived from the comparison of different isochrone sets.

Models	Age	$E(B - V)$	$(m - M)_V$
Yale–Yonsei	1.8 $\pm$ 0.3	0.63 $\pm$ 0.05	11.80 $\pm$ 0.10
Padova	1.8 $\pm$ 0.3	0.57 $\pm$ 0.05	11.75 $\pm$ 0.10

7 A ZOOM OF THE TO REGION: GETTING ADDITIONAL CLUES TO THE BINARY POPULATION

Now that we have determined the cluster's fundamental parameters, we can use the best-fitting isochrone as a tool to investigate possible binaries among cluster members from a purely photometric point of view. In Fig 10 we provide a zoom of the TO region, and indicated with filled circles (colour coded in red) RV members. The solid line is the best-fitting Padova isochrone (see Fig. 9). The dashed curve is the same isochrone, but shifted up by 0.75 mag, to illustrate the locus of unresolved equal-mass binaries. This exercise is suggesting us

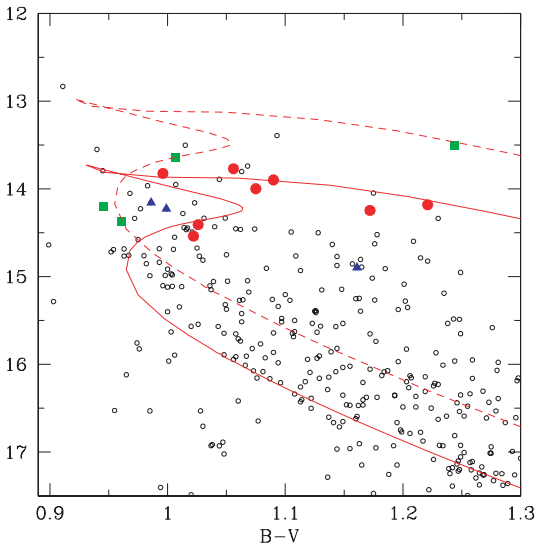

Figure 10. A zoom of the TO region in NGC 2112 CMD. Filled circles indicate bona fide single stars, filled squares indicate possible equal-mass binary systems and filled triangles indicate multiple systems or unequal-mass binaries. The solid line is the best-fitting isochrone which is also shown in Fig. 9, whereas the dashed line is the same isochrone shifted upward by 0.75 mag to mimic the location of equal-mass binaries.

that several stars that lie off the best-fitting isochrone may in reality be unresolved binaries. In fact some of them lie very close to the binary locus, and we indicate them as filled squares (colour coded in green) in the CMD of Fig. 10. They are stars #707, 824, 782 and 601. At the same time, we indicated as filled triangles (blue when printed in colour) stars which lie neither in the single star nor in the binary star sequence. These are stars #714, 707 and 323. One may speculate that these are unequal-mass binaries or may be systems with more than two components. If we refer only to the TO region, we are left with 14 single member stars and seven possibly multiple systems, which implies a rough binary estimate of 33 per cent.

8 DISCUSSION AND CONCLUSIONS

In this paper we presented new photometric and spectroscopic data in the field of the old open cluster NGC 2112. This new data set allowed us to revise the cluster's fundamental parameters and clarify a long-lasting debate on its properties, which for many years, have been poorly constrained due to the high level of field star contamination. By means of multifibre spectroscopy, we measured RV for 40 stars and found 21 RV members. This, in turn, allowed us to clean the CMD, providing a better comparison with stellar models.

The most important result of our study is that the cluster has a metallicity much higher than previous determinations, and somewhat higher than the Sun. Also the α-elements are marginally enhanced with respect to the Sun, but still compatible with the trends of thin-disc stars in the solar vicinity, as are all the other elements we measured.

Therefore NGC 2112 is typical of old, thin-disc star clusters, as metal-rich as the Hyades (Boesgaard & Friel 1990), and located at less than 1 kpc from the Sun in the anticentre direction.

In addition, we confirmed the age of the cluster ($\sim$1.8 Gyr), previously derived on a purely photometric basis (Carraro et al. 2002). As for the distance and reddening, our values are in agreement within the errors of previous determinations.

This study stresses the importance of performing detailed membership analysis in Galactic open clusters in order to derive more robust estimates of their fundamental parameters.

ACKNOWLEDGMENTS

This research was part of a joint project between Universidad the Chile and Yale University, partially funded by the Fundación Andes. Hydra observations were performed remotely from Yale by MVM. CMB acknowledges Universidad de Chile graduate fellowship support from programme MECE Educación Superior UCH0118 and Fundación Andes C-13798. MVM was supported by an NSF Astronomy and Astrophysics Postdoctoral Fellowship, under award AST04-011640. GC thanks Doug Geisler, Tom Richtler and Roberto Barbon for long and interesting discussions on NGC 2112, and the anonymous referee who helped us to improve the paper presentation. This study made use of SIMBAD and WEBDA.

REFERENCES

Alonso A., Arribas S., Martínez-Roger C., 1999, A&AS, 140, 261
Bensby T., Feltzing S., Lundström I., Ilyin I., 2005, A&A, 433, 185
Boesgaard A. M., Friel E. D., 1990, ApJ, 351, 467
Brown J. A., Wallerstein G., Geisler D., Oke J. B., 1996, AJ, 112, 1551 (BWGO96)
Carraro G., Ng Y. K., Portinari L., 1998, MNRAS, 296, 1045
Carraro G., Barbon R., Boschetti C. S., 2002, MNRAS, 336, 259
Carraro G., Villanova S., Demarque P., McSwain M. V., Piotto G., Bedin L. R., 2006, ApJ, 643, 1151
Carraro G., Geisler D., Villanova S., Frinchaboy P. M., Majewski S. R., 2008, A&A, 476, 217
Demarque P., Wo Y., Kim Y., Yi S. K., 2004, ApJS, 115, 667
Dias W. S., Alessi B. S., Moitinho A., Lepine J. R. D., 2002, A&A, 389, 871
Friel E. D., Janes K. A., 1993, A&A, 267, 75 (FJ93)
Friel E. D., Jacobson H. R., Barrett E., Fullton L., Balachendran S. C., Pilachowski C. A., 2003, AJ, 126, 2372
Geisler D., 1987, AJ, 94, 84
Geisler D., Claria J. J., Minniti D., 1991, AJ, 102, 1836
Girardi L., Bressan A., Bertelli G., Chiosi C., 2000, A&AS, 141, 371
Gratton R. G., Carretta E., Eriksson K., Gustafsson B., 1999, A&A, 350, 955
Houdashelt M. L., Bell R. A., Sweigart A. V., 2000, AJ, 119, 1448
Horne K., 1986, PASP, 98, 60
Janes K. A., Phelps R. L., 1994, AJ, 108, 1773
Karatas Y., Schuster W. J., 2006, MNRAS, 371, 1793
Kim Y.-C., Demarque P., Alexander D. R., 2002, ApJS, 143, 499
Kurucz R. L., 1992, in Barbuy B., Renzini A., eds, Proc. IAU Symp. 149, The Stellar Populations of Galaxies. Kluwer, Dordrecht, p. 225
Kurucz R. L., Furenlid I., Brault J., Testerman L., 1984, National Solar Observatory Atlas. National Solar Observatory, Sunspot, New Mexico
Landolt A. U., 1992, AJ, 104, 340
Mermilliod J.-C., Mayor M., 2007, A&A, 470, 919 (MM07)
Richtler T., 1985, A&AS, 59, 491 (R85)
Richtler T., Kaluzny J., 1989, A&AS, 81, 225
Schlegel D. J., Finkbeiner D. P., Davis M., 1998, ApJ, 500, 525
Schmidt-Kaler Th., 1982, in Schaifers K., Voigt H. H., eds, Numerical Data and Functional Relationships in Science and Technology, Landolt-Börbstein, New Series, Group VI, Vol. 2(b). Springer-Verlag, Berlin, p. 14
Stetson P. B., 1987, PASP, 99, 191
Yi S. K., Demarque P., Kim Y.-C., Lee Y.-W., Ree C. H., Lejeune Th., Barnes S., 2001, ApJS, 136, 417
Zacharias N., Urban S. E., Zacharias M. I., Wycoff G. L., Hall D. M., Monet D. G., Rafferty T. J., 2004, AJ, 127, 3043

This paper has been typeset from a TEX/LATEX file prepared by the author.